Renewable Energy 220 (2024) 119684

Contents lists available at ScienceDirect

Renewable Energy

journal homepage: www.elsevier.com/locate/renene

Numerical assessment of tidal potential energy in the Brazilian Equatorial Shelf

Alessandro L. Aguiar [a,b,c,j,*], Martinho Marta-Almeida [g,h], Mauro Cirano [i,j], Janini Pereira [d,f,j], Letícia Cotrim da Cunha [b,c,e]

[a] Departamento de Oceanografia Física e Meteorologia, Faculdade de Oceanografia, Universidade do Estado do Rio de Janeiro, Rio de Janeiro, Brazil
[b] Programa de Pós-graduação em Oceanografia, Faculdade de Oceanografia, Universidade do Estado do Rio de Janeiro, Rio de Janeiro, Brazil
[c] Rede Clima, Sub-rede Oceanos, Instituto Nacional de Pesquisas Espaciais, São José dos Campos, Brazil
[d] Programa de Pós-graduação em Geofísica, Instituto de Geociências, Universidade Federal da Bahia, Salvador, Brazil
[e] Rede Brasileira de Pesquisa em Acidificação dos Oceanos (BrOA), Universidade Federal de Rio Grande, Rio Grande, Brazil
[f] Departamento de Física da Terra e do Meio Ambiente, Instituto de Física, Universidade Federal da Bahia, Salvador, Brazil
[g] Centro Oceanográfico de A Coruña, Instituto Español de Oceanografia, A Coruña, Spain
[h] Centro Interdisciplinar de Investigação Marinha e Ambiental, Universidade do Porto, Portugal
[i] Departamento de Meteorologia, Instituto de Geociências, Universidade Federal do Rio de Janeiro, Rio de Janeiro, Brazil
[j] Rede de Modelagem e Observação Oceanográfica (REMO), Brazil

ARTICLE INFO

Keywords:
Regional modeling
Tidal barrage
Tidal height
Clean energy

ABSTRACT

The Brazilian Equatorial Shelf (BES) is one among the macrotidal regions worldwide. This study used a high-resolution numerical configuration of the ocean model ROMS (Regional Ocean Modeling System) forced with realistic surface and lateral forcing, as well as with tides and river discharges. Tidal heights of more than 2 m were found in three regions in BES due to the large tidal amplification across the estuarine channels inside each region: Amazon, Pará, and Maranhão, and for a considerable time fraction. Heights between 4 and 5 m occurred with a frequency greater than 20%–30% in some regions. All hypothetical barrages proposed in this study were capable of an annual power production, in two-way mode, higher than La Rance (533 GWh year^{-1}, two-way operation, France) and Sihwa (553 GWh year^{-1}, flood-only operation, South Korea), except one with the same production as Sihwa barrage. The installation effort was evaluated using the Gibrat ratio, the ratio between the length of the barrage and its annual energy production. Among the proposed barrages, the most efficient ones have an annual power generation greater than 1500 GWh year^{-1} and a Gibrat ratios between 1.17 and 3.26, much lower than the Gibrat ratio of Sihwa tidal barrage.

1. Introduction

Tides represent a highly predictable resource because they are caused by astronomical oscillatory gravitational forces. This sinusoidal nature of the tidal resource constitutes an advantage over other renewable sources like wind, solar and ocean waves. In the previous century, commercial tidal energy extraction was associated with potential energy due to sea level differences via the construction of tidal barrages. Several bays and estuaries have been studied for their installation and some sites are in operation, mainly in France, UK, Canada and Russia [1,2]. Tidal barrages allow for more control in energy production than tidal stream turbines (e.g., [3]). The environmental impacts are actually the main disadvantage of energy production through tidal barrages (e.g., [4]). For instance, they change or inhibit the residual circulation as well as the sediment dynamics, thus potentially modifying the marine life and water quality. They may also impact marine traffic and activities like fishing and tourism.

There are three main ways of extracting the potential energy of the tides: generation during ebb tide, generation during flood tide and generation throughout the tidal cycle [5]. Ebb tide generation is the simplest way of operating a tidal barrage. Shortly after flood tide, the reservoir filling gates are closed. The energy generation process starts during the ebb tide, when the water fall is approximately half the tidal amplitude, that is, there is enough water level for the turbines to start operating. This operation is maintained until the height of the water becomes the minimum possible for power generation. At this point, the gates through which the water flows toward the turbines are closed, and energy generation is stopped until the height of the water becomes

* Correspondence to: Faculdade de Oceanografia, Universidade do Estado do Rio de Janeiro (UERJ), 20550-900, Rio de Janeiro RJ, Brazil.
E-mail address: aguiar.alessandro@uerj.br (A.L. Aguiar).

https://doi.org/10.1016/j.renene.2023.119684
Received 16 January 2023; Received in revised form 20 September 2023; Accepted 16 November 2023
Available online 17 November 2023

sufficient for the turbines to operate again, after the next flood tide. The generation process during flood tide is similar to that during ebb tide, except that the tidal generation occurs in the sea-reservoir direction. The generation during the whole cycle is, therefore, the combination of the generation during ebb tide and during flood tide [5].

The installation of a tidal barrage brings environmental and socioeconomic impacts which are unique for each location. The viability of the project also has technical constrains. Factors to take into account include bed morphology, water depth, distance to coast, ports, main shipping routes and lightering zones, grid connection feasibility, operation and maintenance coasts of the energy converters subjected to biofouling and corrosion. Also, the devices (turbines) to installed in the tidal barrages must be tested in terms of ability to resist the turbulence, wave interactions and velocity shear across its moving parts (e.g., [6,7]). Appropriate resource and impact assessments are required to understand its positive and negative consequences [8]. For instance: changes in sediment transport patterns may decrease the turbidity; a reduction in tidal currents may decrease the vertical mixing; the salinity structure and the availability of dissolved oxygen can be modified as well as the resuspension of metals and the concentration of nutrients and pathogens [9]. The alteration of the living conditions of marine species, including the nursery, recruitment and settlement regions are a consequence of modifications in physical conditions like the wave/tidal regime, sediment concentration and water column turbidity [10,11]. These environmental issues are not restricted to the tidal barrage site but can be felt several kilometers away [12–16]. This means that there should exist a good knowledge of the area at the regional scale prior to the installation of tidal barrages.

In Brazil, the use of renewable energy accounts for 48% of all available energy in the country [17]. If the generation of electricity is considered separately, renewables account for almost 80% of the energy produced, out of which about 72% is related to hydroelectricity; 14%, 11% and 3% are related to wind, biomass fuel, and solar energy respectively [18]. According to International Energy Agency [19], the Levelized Cost of Energy (USD/MWh) of non-pollutant renewable energy (wind: 33.59; solar 46.02; hydro: 46.12) is lower than that of energy from combustion (biomass: 53.52; gas: 78.89; coal: 96.94) in Brazil. Yet, ocean energy extraction is not considered in the investment perspectives of the Brazilian Development Bank for 2018–2021 [20]. Likewise, no mention is given to future ocean energy production in the Decadal Plan for Energy Expansion 2031 [17]. Despite the lack of government interest in ocean energy, a joint venture between federal and private institutions installed a prototype of a 50 kW hyperbaric wave energy converter in 2012 in the State of Ceará, Northeast Brazil [21]. The first Brazilian tidal power plant was intended to be installed in Bacanga estuary in the State of Maranhão, Northeast Brazil, capable of producing about 44 GWh per year [22]. Even though this project was proposed since the barrage was built about 40 years ago, it was not implemented due to the lack of investment on infrastructure, equipment and research.

Most tidal energy assessment studies in Brazil (e.g., [22,23]) are based on data of tidal harmonic components obtained from a port close to the tidal barrage location, which are synchronized to a tide table provided by Brazilian Navy. This approach may be appropriated for a first and local assessment of energy. However, as tides are modulated by the interaction with bathymetry and sea level time series can be influenced by phenomena not included in tidal components as local wind effects and meteorological tides, tidal energy studies should thus consider the tidal heights in the tidal barrage site and be done on a long-term basis. In this way, the present work aims to assess the potential of energy extraction from tidal heights based on a high-resolution and long-term model simulations using realistic forcings over the Brazilian Equatorial Shelf (BES), where the greatest tidal amplitudes (in excess of 3 m [22,24]) are observed in the country. This knowledge is a necessary basis for planning and decision making on installation of tidal barrages as well as the evaluation of the associated impacts.

2. Regional setting

The BES is part of the northern coast of South America. This region hosts the river with the world largest freshwater discharge: the Amazon River [25,26]. The BES is subject to energetic forcings, including resonant semidiurnal macrotides, large buoyancy flux from the Amazon River, northeasterly and southeasterly trade winds, and intense flow along the continental margin associated with the NBC. These forcings also perform an important role in the dispersion of the Amazon freshwater discharge and associated suspended sediment [27,28]. In addition to BES having such unique features, its circulation plays a key role in the interhemispheric exchange of fresh water [29], heat and energy [30,31], having thus a relevant influence on global ocean circulation.

The study area is located between latitudes 8°S and 10°N and longitudes 30°W and 56°W (Fig. 1) and its width varies significantly. South of 3°S, the shelf is narrow and covered by carbonate sediments [32]. North of 3°S, the BES widens to 100–300 km near the Amazon River where fluid mud is present. The BES houses the Amazon Continental Shelf (ACS), a smaller region between latitudes 1°S and 5°N and longitudes 52°W and 43°W, which is under direct influence of the Amazon River. Despite the marked salinity anomalies relative to the large river discharge, the ACS circulation is driven by other forcings [24]. Located at the equator, the ACS circulation is subject to a geostrophic degeneracy and terms other than Coriolis are responsible for the momentum balance: advection, wind stress, and pressure gradient. This promotes a faster dynamic response compared to regions where geostrophy is important [33].

Tides on the ACS are mainly forced by the deep ocean tides [24]. Tides propagate to shallower regions having its properties modified by friction, conservation, and resonance processes. The semidiurnal tidal components (M_2, S_2, N_2) are generally known as dominant in the equatorial Atlantic Ocean [25], with strong fortnightly modulations (spring/neap tides). The ACS response to semidiurnal ocean forces is quite complex, due to the Amazon mouth and the shelf bathymetries. The M_2 tidal wave propagates perpendicular to the coast toward the Amazon and Tocantins rivers, and influences the Amazon river mouth and the ACS between 1°N and 4°N. In this region, M_2 reaches a maximum amplitude in excess of 3 m for the nearshore area, where the shelf width is maximum, generating quasi-resonant conditions [24]. Beardsley et al. [34] showed that the M_2 is an important forcing of the ACS circulation, responsible for about 70% of the tidal variability, inducing strong currents (reaching 2 m s^{-1} during spring tides) and elevations with amplitude exceeding 1.5 m near the coast. The M_2 amplitude increases to 1.75 m at about 2°N [33]. Diurnal tides in the ACS, mainly K_1 and O_1, have much smaller amplitudes, ranging from 0.06 to 0.08 m over the shelf. Therefore, in a region with such strong tidal currents, a numerical assessment of the tidal stream energy is needed to the better understanding of the BES potential to generate clean and renewable energy.

3. Data and methods

3.1. Model setup

The ocean simulations were performed using the Regional Ocean Modeling System (ROMS). ROMS is a 3D model that solves the free-surface, hydrostatic, primitive equations of the ocean over a variable topography [35,36]. On the horizontal, the model uses orthogonal curvilinear coordinates with Arakawa C grid and adopts stretched terrain-following coordinates in the vertical. The model uses a split-explicit time stepping scheme which provides a great computational efficiency [37]. A detailed description of the model algorithms can be found in [35,38,39].

The simulations were performed for a five-year period, 2009 to 2013. The simulations started earlier on September 2008, as a 4-month model spin-up. The grid has horizontal resolution of 1/24° (~4.2

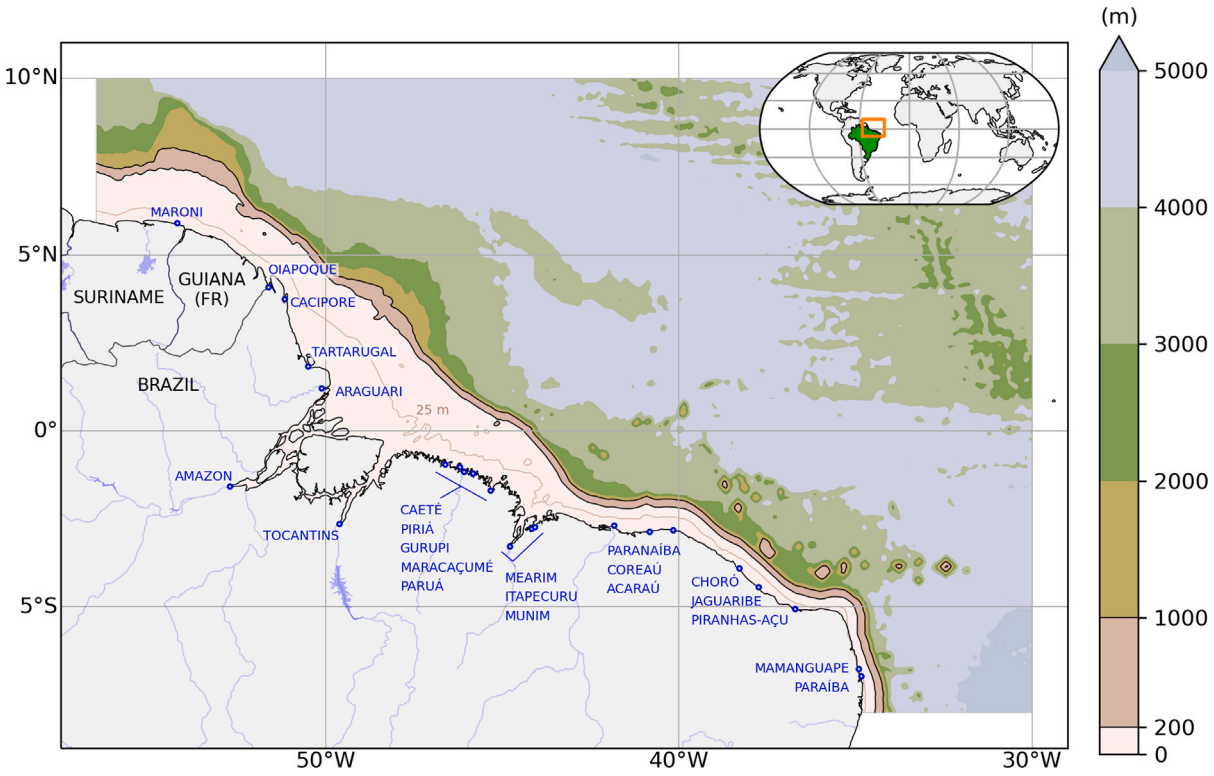

Fig. 1. Bathymetry and model domain. The light brown line indicates the 25 m isobath. The blue circles indicate the location where the discharge of each river was included in the model configuration. The inset world map shows Brazil in green and the model domain in orange.

km) and 32 vertical levels. The domain covers the latitudes 8°S and 10°N and longitudes 56°W and 30°W, extending ~2000 km in north–south direction and ~2900 km in east–west direction (Fig. 1). The topography derives from very high resolution bathymetric surveys held by the Brazilian Navy over the Amazon shelf and ETOPO1 [40], with a resolution of an arc-minute (about 1.8 km).

The Amazon shelf has a highly variable bottom friction due to spatial differences in the sediment characteristics, including the presence of fluid mud. Since tidal dynamics is strongly modulated by bottom friction, the rugosity length spatial map for the region proposed by Le Bars et al. [41] was adopted. Away from the Amazon shelf, the typical value of 1 cm was used for bottom roughness, decreasing to 0.01 and 0.005 cm roughly inside isobath 25 m in front and north of Amazon river mouth (also 0.01 cm at the São Marcos Bay in the state of Maranhão, see Fig. 5 in [42]).

Offline nesting was done with the 1/12° solution of the HYbrid Coordinate Ocean Model (HYCOM) (Version 2.2) from the National Consortium for Data Assimilative Modeling (NCODA) [43]. HYCOM/NCODA provided initial and daily lateral boundary conditions (temperature, salinity, sea level, and currents). Tracers (temperature and salinity) and 3D velocity were set at the boundaries using active/passive radiative conditions [44]. Chapman [45] and Flather [46] boundary conditions were adopted for sea level and 2D velocity respectively.

Tidal forcing was obtained from the TPXO global database [47], version 7.2, which provides the amplitudes and phases of sea surface elevation and barotropic currents of the main semidiurnal and diurnal tides components (M_2, S_2, N_2, K_2, K_1, O_1, P_1, Q_1) and two long period components (M_f, M_m), with spatial resolution 1/12°.

The variables for the calculation of the air-sea fluxes (humidity, pressure, temperature, precipitation, radiation and wind) were derived from the Climate Forecast System Reanalysis (CFSR, [48]). CFSR is the third generation of the reanalysis products from the National Center for Atmospheric Research (NCAR/NOAA), with spatial resolution at the surface of 0.25° and temporal resolution of 6 h.

Rivers were included as monthly climatologies which were calculated based on measurements taken by ANA (Portuguese acronym for National Waters Agency), following Dai et al. [49]. All rivers included are indicated in Fig. 1. The Amazon and Tocantins rivers are the largest rivers in the region with 91% and 6% of the total discharge of all the rivers respectively. The annual average flow of these rivers is 183×10^3 m^3 s^{-1}, with a seasonal amplitude of 60 m^3 s^{-1} and 13 m^3 s^{-1} for Amazon and Tocantins rivers respectively. Amazon River reaches a maximum discharge in May and minimum in November, while Tocantins River has a maximum discharge by March/April and minimum between August and October.

Model outputs were validated against daily *in situ* temperature profiles from PIRATA (Pilot and Research Array in the Tropical Atlantic, [50]), sea surface temperature reanalysis from MUR SST (Multi-scale Ultra-high Resolution Sea Surface Temperature, [51]) and sea surface height reanalysis from AVISO (Archivage, Validation et Interprétation des données des Satellites Océanographiques, [52]), and hourly tidal heights records from GLOSS (Global Sea Level Observing System)'s Fortaleza station (3.72°S, 38.47°W) considering the entire period of simulation (five years). Validation against MUR SST and AVISO reanalyses showed RMSE values up to 0.75 °C and 0.14 m in most of the domain respectively. Validation against PIRATA's P1, P2 and, P3 buoys, showed that modeled profiles in general laid within the standard deviation limit. Regarding tidal validation, the largest difference for the main tidal constituent in the region, M_2, between modeled and GLOSS amplitude and phase were of 0.03 m and 0.85° respectively. For further details on the model configuration and the validation, please see [42].

3.2. Evaluation of energy potential

The time series of modeled tidal heights have hourly time resolution and were used to calculate the tidal energy.

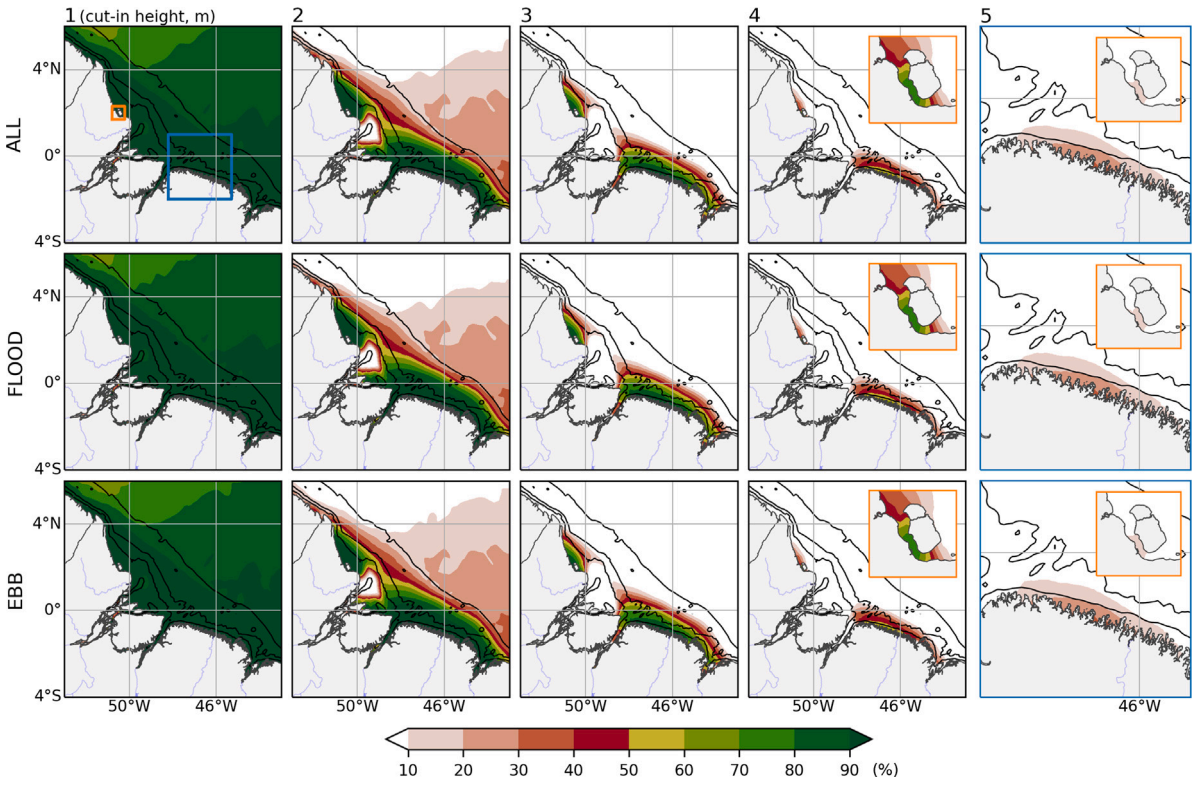

Fig. 2. Spatial distribution of the percentage of tidal heights (semi-cycles) greater than the cut-in values of 1, 2, 3, 4 e 5 m. Results are shown for the whole tidal cycle (ALL), flood, and ebb respectively. The isobaths 10, 25 and 200 m are also illustrated in each panel. The blue rectangle in the first panel (upper left) shows the zoom region depicted in the right panels (cut-in 5) and the small orange rectangle represents the zoom region inset in the two rightmost columns (cut-in 4 and 5).

The potential energy (J) of a filled tidal barrage is given by:

$$E = \frac{1}{2}\rho g A H^2 \tag{1}$$

where ρ is the water density (1024 km m^3), g is the acceleration of gravity (9.81 m s^{-2}), A is the area of the barrage (m^2) and H is its height (m, the difference between high and low tide).

During a period T (s) during which the barrage fills N times, the power density (W m^{-2}) is given by:

Potential power density (W m^{-2})

$$P = \frac{1}{T}\sum_{i=1}^{N}\frac{1}{2}\rho g H_i^2 \tag{2}$$

The Gibrat Ratio (e.g., [53]) is the ratio between the length of the dam, L (m), and the amount of stored energy at the dam (MWh):

$$G = \frac{L}{E10^{-6}/3600} \tag{3}$$

Thus, this ratio provides a first idea of the cost-effectiveness of installing a dam.

Since tidal barrages require a minimum height, some results will be shown as a function of their respective cut-in values.

4. Results

4.1. Spatial variability

Fig. 2 shows the percentage of time, considering the entire simulated period, in which tidal heights are higher than the selected cut-in values (from 1 to 5 m). Heights less than the cut-in value were zeroed in the time series. These results provide an initial view of the regions where the highest and most frequent tidal heights occur. In Fig. 2, the heights during flood, ebb and the entire tidal cycle are shown in order to analyze the conditions of single and double effect tidal generation (two-way, both during the ebb and the flood). A similar pattern of height distribution can be seen during the flood, ebb and the entire tidal cycle. Across the study area, heights of 2 m are observed during more than 70% of the time. The highest heights are observed north of the Amazon mouth, along coast (Amazon adjacent region, AM_{adj} hereinafter), on the coast of Pará and Maranhão (PAMA) and in Maranhão (MA, by the longitude 44.5°W). In AM_{adj} and MA, heights between 4 and 5 m occurred with a frequency greater than 30% while, in PAMA, heights above 5 m are observed in 20 to 40% of the period of the simulation.

The spatial distribution of the power density available at the height of the tides, averaged over the simulation period and calculated based on Eq. (2), is shown in Fig. 3. Different cut-in heights were also taken into account, from 1 to 5 m and estimates were made for the flood, ebb or the entire sea cycle, analogously to the analysis shown in Fig. 2. Using the cut-in height of either 0 and 1 gave approximately the same results as most of tidal heights in the region are greater than 1 m as shown in Fig. 2. A similar pattern of height distribution is observed during the flood, ebb and the entire tidal cycle. However, when considering the two-way generation, the power density values are about the double (4×10^3 W m^{-2}) of the values considering only the flood or ebb. In other words, the energy available when tidal extraction can be done in both flood and ebb approximately doubled. The actual energy extracted may not be the double due to difference in two-way and one-way turbine efficiencies. The spatial pattern of the power density values is practically identical for cutting heights from 0 to 2 m. From the cut-in value of 3 m, the 3 regions AM_{adj}, PAMA and MA stand out. Above the cut-in height of 5 m, energy is only available in PAMA and a small portion of AM_{adj}.

4.1.1. Tidal barrages

To have a more quantitative idea of the tidal generation potential via potential energy, tidal generation for hypothetical tidal barrages

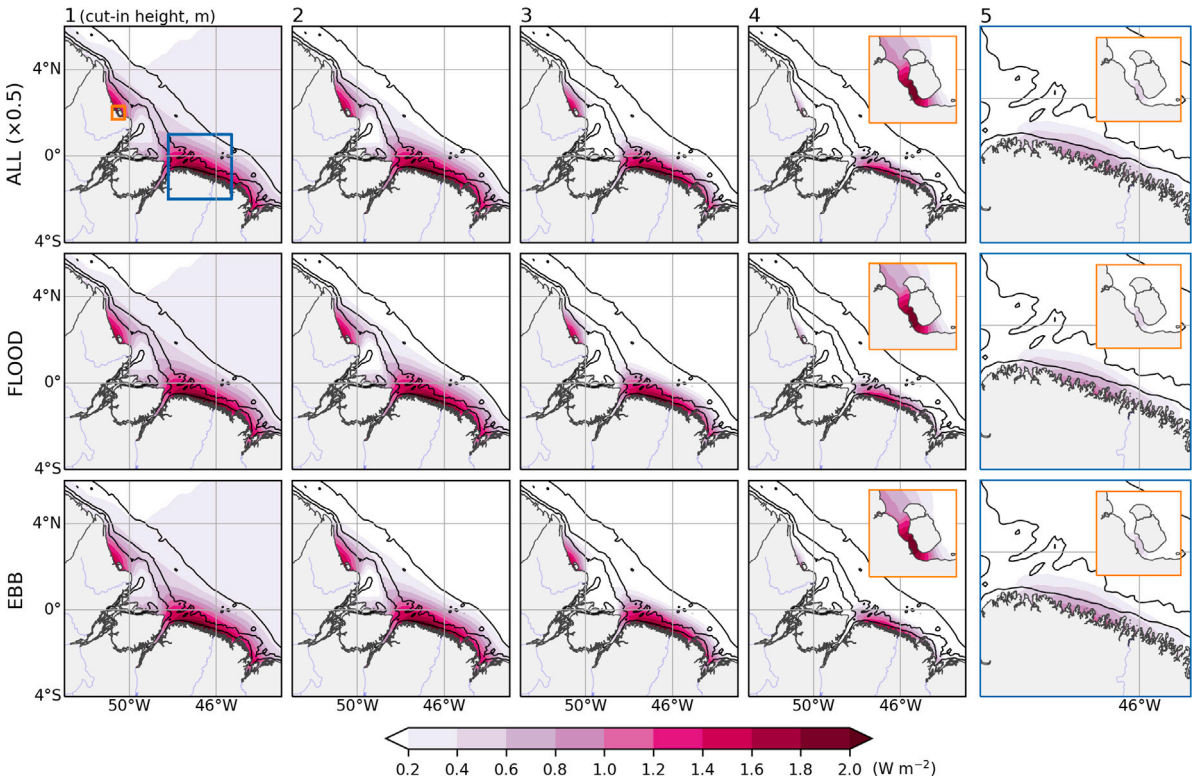

Fig. 3. Time averaged power density of tidal heights ($\times 10^3$ W m^{-2}) calculated considering the whole tidal cycle (ALL), flood, and ebb heights. Results using cut-in heights ranging from 1 to 5 m are shown in each column. The isobaths 10, 25 and 200 m are also illustrated in each panel. The blue rectangle in the first panel (upper left) shows the zoom region depicted in the right panels (cut-in 5) and the small orange rectangle represents the zoom region inset in the two rightmost columns (cut-in 4 and 5). The values of the top panels were halved to fit the color mapping limits.

along the study area was calculated. For this estimate, areas were established for each proposed tidal barrage. The determination of the location and area of the barrages was based on the following criteria: (i) values and frequency of tidal heights (Fig. 2); (ii) power density (Fig. 3); (iii) barrage length; and (iv) taking advantage of the natural continental contours (e.g., embayments, estuarine channels and indentations along the coast). Such criteria were established with the aim of enabling a greater production of clean energy (criteria i and ii) and at the same time with lower installation, operation and maintenance costs (criteria iii and iv). Thus, the location hypothetical barrages was determined considering the sites where the greatest tidal heights occur during the highest percentage of time in the simulation period (criterion i) and where the largest power density was observed (criterion ii). Concerning energy generation in tidal barrages, the larger the barrage area is, more energy is produced and the shorter the barrage length, the lower the installation costs. Thus, the choice of the location and area of each proposed barrage considered the continental contours so that the largest amount of water could be held in a reservoir with the shortest barrage length (criteria iii and iv). In Fig. 4 the barrages chosen for the 3 regions are indicated (AM_{adj}, PAMA and MA).

Fig. 5 shows the temporal variability, in terms of box plots, of tidal energy production for each tidal barrage, also considering its mode of operation (flood-only, ebb-only and two-way generation). Tidal energy projects are characterized by low levels of power conversion efficiency, usually ranging from 20% to 40%, with an average of 33% often being used [54]. During two-way generation, turbines that have the capacity to be bi-directional are used. In this case, turbine efficiency is reduced as turbines also operate in reverse mode [3]. Thus, to estimate the potential energy extracted from the tides, a turbine efficiency value of 0.33 (33%) was used for generation in ebb-only and flood-only modes, and the minimum value, 0.20 (20%), was used for two-way generation. The barrages with the highest power production are $AM_{adj}1$ and 2 followed by PAMA3, PAMA7 and MA1 and 2. This same pattern appears when analyzing the variability of power generation of each barrage. The barrages in AM_{adj} are in the same location, however, they are proposed barrages with dimensions that cover different areas. The same applies to PAMA3 and 4. $AM_{adj}1$ can operate with 600 MW over a tidal cycle, representing an annual production of 5000 GWh. However, this production only occurs in 5% of the tidal elevations ranges (during both flood and ebb). Nevertheless, the median power exceeds 400 MW. In PAMA region, PAMA3 and PAMA7 stand out in relation to other sites with median power around 200 MW. PAMA4 (169.3 km^2), even though it is in the same estuary as PAMA3 (465.5 km^2), but with an area about 3 times smaller, it has a much lower tidal production, similarly to other barrages in the PAMA region. Interestingly, the MA1 and MA2 barrages, even with very different tidal heights, present a very similar power generation, both on average and considering temporal variability.

5. Discussion

After assessing the availability and possibilities of power extraction via tidal heights in the study area, it is worth discussing the tidal power generation quantitatively and the applicability of the extraction strategies presented in Section 4.1.1. For this purpose, the average of the total energy production per year was calculated, taking into account turbine efficiencies (0.33 for ebb-only and flood-only modes and 0.2 for the two-way generation) and compared with current installations, either already working actively (i.e., La Rance, two-way operation, France, and Sihwa, flood-only operation, South Korea) or still in planning (i.e., Severn, ebb-only operation, United Kingdom). The results are shown in Table 1. $AM_{adj}1$ and 2, PAMA3 and 7, and MA2 and 1 are capable of producing the highest energy values. On the other hand, the barrages with the lowest annual performance are in the PAMA region, namely: PAMA2 and 6. In addition, another important finding is that in the two-way operation mode (generation during both flood and ebb), the tidal generation is approximately 21% higher, although there is a

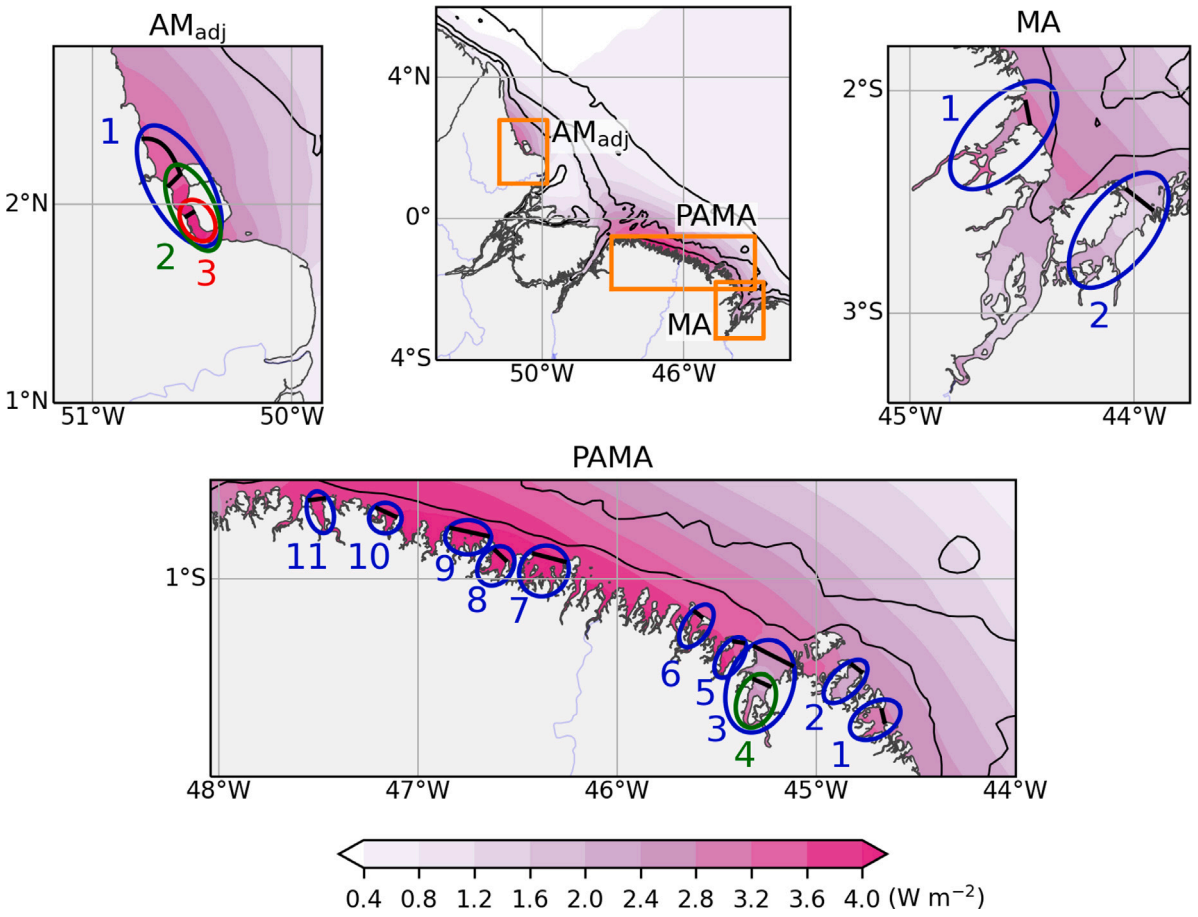

Fig. 4. Time averaged power density of tidal heights (10^3 W m^{-2}) calculated considering the whole tidal cycle. The proposed tidal barrages are indicated by the ellipses in their respective region. The black contours shown indicate the isobaths 10, 25 and 200 m.

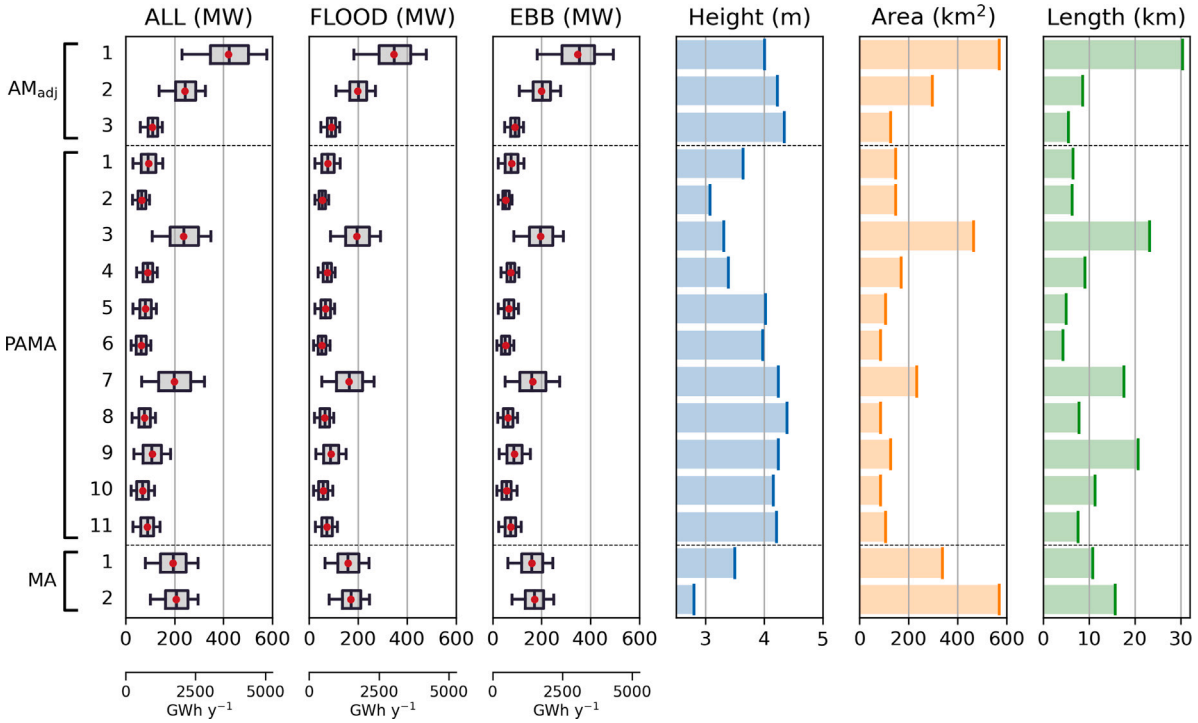

Fig. 5. Boxplots of energy production (GWh) of the proposed tidal barrages in the study area. Results are shown for the whole tidal cycle (ALL), flood, and ebb respectively. The lower and upper limits of the box plots are the percentiles 5 and 95%. The red dot inside the interquartile range rectangle indicates the mean and the vertical line represents the median. Also shown the average tidal height (of both flood and ebb), area and length of the barrages in the three rightmost panels.

reduction in the efficiency of the turbine operating in both directions. Considering only the single operation mode, it is observed that the difference between flood-only and ebb-only modes are in general very small in all the proposed tidal barrages. All the barrages proposed in this study are capable of producing energy in two-way mode higher than La Rance (533 GWh year^{-1}) and Sihwa (553 GWh year^{-1}), except PAMA6 with the same production as Sihwa (553 GWh year^{-1}).

The values of energy are greatly influenced by the area of the tidal barrage, generally in the order of km^2 (10^6 m^2). However, it is known that the larger the size of the barrage, the greater the installation and maintenance costs, in addition to requiring a more accurate study of the structure's resistance and impacts on the environment. Thus, to assess the feasibility of a tidal barrage project, estimating its annual production is not a sufficient criterion for decision making.

A first guess regarding a tidal barrage cost and efficiency is given by the Gibrat ratio (Eq. (3)), which consists on the ratio between the barrage length and its potential energy content when filled. The Gibrat ratios of the proposed tidal barrages in given in the 5th column of Table 1. The most viable installation barrages were $AM_{adj}2$ followed by $AM_{adj}3$ and MA1. The least viable are PAMA9 and 10. It is worth to note that while the Gibrat ratios of all the barrages in this work are higher the ratios of La Rance and Severn, they are much lower than the ratio for the South Korean barrage of Sihwa, and some are comparable to the ratio of Severn, around 1. From this analysis, we can infer that the barrages with the highest annual tidal production and the most viable installation are $AM_{adj}1$ and 2, PAMA3 and 7, and MA1 and 2, all with annual energy output greater than 1500 GWh and Gibrat ratios between 1.17 and 3.26. Thus, among the proposals, there are barrages with great energy potential and viable in the 3 regions considered for the conversion of tidal potential energy into electrical energy in the study area.

These findings reveal important features of tidal energy generation in BES. However, it is important to keep in mind that this is a preliminary study for this region. Due to resolution limitations, narrow channels could not be represented, which may have some implications in the evaluation of the potential in generating tidal energy in the region. For instance, along narrow channels tides may be even more amplified, thus tidal amplification might have been underestimated in some regions. Analogously, barrage area might also been underestimated, reducing the energy output estimated. In addition, the model may represented these narrow channels as land and, in some cases, more than one barrage would be needed to build the reservoir.

6. Summary and conclusions

A numerical assessment study of the tidal stream power density was conducted for BES, one among the macrotidal regions worldwide and that also hosts the largest estuary of the Brazilian coast in Maranhão state. The model simulations were based on a configuration described in [42], which was validated against temperature and salinity profiles, as well as free surface at tidal and sub-tidal time scales. This was the first modeling configuration created for the region using realistic lateral and surface forcing, besides tides and riverine input.

Tidal generation for hypothetical tidal barrages was estimated. The barrages with the highest power production are $AM_{adj}1$ and 2 followed by PAMA3 and MA1 and 2 (see Fig. 4 for the locations). $AM_{adj}1$ can operate with a peak power output of 600 MW, which occurs during 5% of the tidal elevations ranges (during both flood and ebb). Median and mean values are still high, above 400 MW, representing an average annual production higher than 3500 GWh. Interestingly, tidal barrages, even with different tidal heights, can present a similar power generation, both on average and considering temporal variability.

Based on the average annual production of tidal power, in the two-way operation mode (generation during both flood and ebb), the tidal generation is approximately 21% higher than in the other modes. All hypothetical barrages proposed in this study were capable of an annual power production, in two-way mode, higher than La Rance (533 GWh year^{-1}, two-way operation, France) and Sihwa (553 GWh year^{-1}, flood-only operation, South Korea), except one with the same production as Sihwa barrage.

Table 1
Annual energy production obtained through the potential energy of tidal heights. H indicates the average height in the simulation period inside the barrage, L the barrage length and A the barrage area. Values related to La Rance, Sihwa and Severn were obtained in literature (e.g., [55,56]).

	H (m)	A (km^2)	L (km)	Gibrat ratio	E (GWh year^{-1})		
					All	Flood	Ebb
$AM_{adj}1$	4.0	571	30.4	2.37	3 677	3 034	3 041
$AM_{adj}2$	4.2	296	8.6	1.17	2 113	1 742	1 745
$AM_{adj}3$	4.3	127	5.5	1.65	959	791	792
PAMA1	3.6	148	6.5	2.39	814	671	672
PAMA2	3.1	148	6.3	3.25	569	470	469
PAMA3	3.3	466	23.2	3.26	2 068	1 708	1 705
PAMA4	3.4	169	9.1	3.36	784	646	647
PAMA5	4.0	106	5.0	2.10	701	579	579
PAMA6	4.0	85	4.3	2.32	553	456	457
PAMA7	4.2	233	17.6	3.01	1 733	1 429	1 431
PAMA8	4.4	85	7.8	3.43	670	553	553
PAMA9	4.2	127	20.7	6.50	950	783	784
PAMA10	4.2	85	11.3	5.55	608	502	502
PAMA11	4.2	106	7.6	2.92	772	637	637
MA1	3.5	339	10.8	1.87	1 690	1 395	1 393
MA2	2.8	571	15.7	2.51	1 810	1 493	1 495
La Rance	8.5	22.5	0.7	0.36	533.0	–	–
Sihwa	5.6	30.0	12.7	9.64	–	553.0	–
Severn	7.5	570.0	16.1	0.92	–	–	15 600

Installation effort was evaluated using the Gibrat ratio. The barrages with the highest annual tidal production and the most viable installation are $AM_{adj}1$ and 2, PAMA3 and 7, and MA1 and 2, all with annual energy production greater than 1500 GWh and Gibrat rations between 1.17 and 3.26, much lower than the Gibrat ratio of the South Korean Sihwa tidal barrage. Thus, among the proposals, there are barrages with great energy potential and viable in the study area.

Finally, from the interpretation of the results presented in this study, it can be seen that the Brazilian Equatorial Shelf is a source of clean energy to be explored. Considering the extraction of energy from tidal heights, it is possible to produce renewables along the entire extension of BES. This sheds a new light in the current humankind scenario, with the depletion of non-renewable energy sources and the need to replace polluting forms of energy production such as the burning of fossil fuels and nuclear plants with clean and renewable generation.

Further research is needed in terms of model simulations with: (i) finer resolutions, with more detailed bathymetry and coastline, and (ii) the implementation of wetting and drying algorithms to represent the variability of inundation areas in intertidal zones; so that the many narrow in the region can be investigated and tidal amplification can be estimated more accurately. Furthermore, future works on the optimization of tidal barrages in BES, the role of high frequency tidal components, namely overtides, and tidal asymmetry on the resource (e.g., [57,58]) are also needed. Moreover, the assessment of the environment consequences of the installation of the proposed tidal barrages in the region is a crucial point to the decision making concerning the sustainable way to better extract tidal potential energy in BES.

CRediT authorship contribution statement

Alessandro L. Aguiar: Conceptualization, Methodology, Investigation, Writing – original draft, Visualization. **Martinho Marta-Almeida:** Conceptualization, Methodology, Investigation, Visualization, Writing – review & editing. **Mauro Cirano:** Supervision, Writing – review & editing. **Janini Pereira:** Supervision, Writing – review & editing. **Letícia Cotrim da Cunha:** Supervision, Writing – review & editing.

Declaration of competing interest

The authors declare that they have no known competing financial interests or personal relationships that could have appeared to influence the work reported in this paper.

Acknowledgments

This work was financially supported by PETROBRAS, Brazil and the Brazilian oil regulatory agency ANP (Agência Nacional de Petróleo, Gás Natural e Biocombustíveis), within the special participation research project Rede de Modelagem e Observação Oceanográfica (REMO). Research grants (no: 151427/2020-8 and 380293/2022-6) were offered by the Brazilian Conselho Nacional de Desenvolvimento Científico e Tecnológico (CNPq). Research grant no: 380293/2022-6 was within the scope of the project Rede Brasileira de Pesquisas sobre Mudanças Climáticas Globais (Rede Clima). M. Marta-Almeida was supported by European Union Atlantic Area Interreg project iFADO (EAPA/165_2016) and by project BlueForesting (PT-INNOVATION-0077) financed by the EEA Grants. Letícia Cotrim da Cunha acknowledges the following research grants: CNPq/PQ-2 309708/2021-4 from Brazilian Conselho Nacional de Desenvolvimento Científico e Tecnológico (CNPq); FAPERJ/CNE SEI260003/003524/2022 from Fundação de Amparo à Pesquisa do Estado do Rio de Janeiro (FAPERJ); and UERJ Prociência 2021–2024.

References

[1] S. Neill, A. Angeloudis, P. Robins, I. Walkington, S. Ward, I. Masters, M. Lewis, M. Piano, A. Avdis, M. Piggott, G. Aggidis, P. Evans, T. Adcock, A. Zidonis, R. Ahmadian, R. Falconer, Tidal range energy resource and optimization - past perspectives and future challenges, Renew. Energy 127 (2018) 763–778, http://dx.doi.org/10.1016/j.renene.2018.05.007.

[2] F. O'Rourke, F. Boyle, A. Reynolds, Tidal energy update 2009, Appl. Energy 87 (2) (2010) 398–409, http://dx.doi.org/10.1016/j.apenergy.2009.08.014.

[3] A. Angeloudis, R. Ahmadian, R.A. Falconer, B. Bockelmann-Evans, Numerical model simulations for optimisation of tidal lagoon schemes, Appl. Energy 165 (2016) 522–536, http://dx.doi.org/10.1016/j.apenergy.2015.12.079.

[4] J. Zhou, R.A. Falconer, B. Lin, Refinements to the EFDC model for predicting the hydro-environmental impacts of a barrage across the Severn Estuary, Renew. Energy 62 (2014) 490–505, http://dx.doi.org/10.1016/j.renene.2013.08.012.

[5] P.B.L. Neto, O.R. Saavedra, N.J. Camelo, L.A.S. Ribeiro, R.M. Ferreira, Exploração da energia maremotriz para geração de eletricidade: Aspectos básicos e principais tendências, Ingeniare. Rev. Chilena De Ingeniería 19 (2) (2011) 219–232, http://dx.doi.org/10.4067/S0718-33052011000200007.

[6] A.S. Bahaj, Generating electricity from the oceans, Renew. Sustain. Energy Rev. 15 (7) (2011) 3399–3416, http://dx.doi.org/10.1016/j.rser.2011.04.032.

[7] M. Mueller, R. Wallace, Enabling science and technology for marine renewable energy, Energy Policy 36 (12) (2008) 4376–4382, http://dx.doi.org/10.1016/j.enpol.2008.09.035.

[8] G. Dalton, G. Allan, N. Beaumont, A. Georgakaki, N. Hacking, T. Hooper, S. Kerr, A.M. O'Hagan, K. Reilly, P. Ricci, W. Sheng, T. Stallard, Economic and socio-economic assessment methods for ocean renewable energy: Public and private perspectives, Renew. Sustain. Energy Rev. 45 (2015) 850–878, http://dx.doi.org/10.1016/j.rser.2015.01.068.

[9] M. Kadiri, R. Ahmadian, B. Bockelmann-Evans, W. Rauen, R. Falconer, A review of the potential water quality impacts of tidal renewable energy systems, Renew. Sustain. Energy Rev. 16 (1) (2012) 329–341, http://dx.doi.org/10.1016/j.rser.2011.07.160.

[10] E.G.A. Carvalho, C.J.C. Blanco, A.A.A.M. Duarte, L.M.F. Maués, Decision support system for hydro power plants in amazon considering the cost of externalities, Int. J. Energy Econ. Policy 10 (2) (2020) 40–47, http://dx.doi.org/10.32479/ijeep.8746.

[11] M.A. Shields, D.K. Woolf, E.P. Grist, S.A. Kerr, A. Jackson, R.E. Harris, M.C. Bell, R. Beharie, A. Want, E. Osalusi, S.W. Gibb, J. Side, Marine renewable energy: The ecological implications of altering the hydrodynamics of the marine environment, Ocean Coast. Manag. 54 (1) (2011) 2–9, http://dx.doi.org/10.1016/j.ocecoaman.2010.10.036.

[12] R. Ahmadian, R. Falconer, B. Bockelmann-Evans, Far-field modelling of the hydro-environmental impact of tidal stream turbines, Renew. Energy 38 (1) (2012) 107–116, http://dx.doi.org/10.1016/j.renene.2011.07.005.

[13] S.P. Neill, J.R. Jordan, S.J. Couch, Impact of tidal energy converter (TEC) arrays on the dynamics of headland sand banks, Renew. Energy 37 (1) (2012) 387–397, http://dx.doi.org/10.1016/j.renene.2011.07.003.

[14] S.P. Neill, E.J. Litt, S.J. Couch, A.G. Davies, The impact of tidal stream turbines on large-scale sediment dynamics, Renew. Energy 34 (12) (2009) 2803–2812, http://dx.doi.org/10.1016/j.renene.2009.06.015.

[15] V. Ramos, R. Carballo, M. Sanchez, M. Veigas, G. Iglesias, Tidal stream energy impacts on estuarine circulation, Energy Convers. Manage. 80 (2014) 137–149, http://dx.doi.org/10.1016/j.enconman.2014.01.027.

[16] J. Thiébot, P. Bailly du Bois, S. Guillou, Numerical modeling of the effect of tidal stream turbines on the hydrodynamics and the sediment transport – Application to the Alderney Race (Raz Blanchard), France, Renew. Energy 75 (2015) 356–365, http://dx.doi.org/10.1016/j.renene.2014.10.021.

[17] Ministério de Minas e Energia, Plano Decenal de Expansão de Energia 2031, 2022, URL https://www.epe.gov.br/sites-pt/publicacoes-dados-abertos/publicacoes/Documents/PDE%202031_RevisaoPosCP_rvFinal_v2.pdf.

[18] Ministério de Minas e Energia, Balanço energético nacional 2022, 2022, URL https://www.epe.gov.br/sites-pt/publicacoes-dados-abertos/publicacoes/PublicacoesArquivos/publicacao-675/topico-638/BEN2022.pdf.

[19] International Energy Agency, Levelised cost of electricity calculator, 2023, URL https://https://www.iea.org/data-and-statistics/data-tools/levelised-cost-of-electricity-calculator.

[20] Banco Nacional de Desenvolvimento, Perspectivas do investimento 2018–2021, 2018, URL https://web.bndes.gov.br/bib/jspui/bitstream/1408/15580/1/Perspectivas_Investimento_2018-2021_Final_P.pdf.

[21] P. Garcia-Rosa, J. Cunha, F. Lizarralde, S. Estefen, I. Machado, E. Watanabe, Wave-to-wire model and energy storage analysis of an ocean wave energy hyperbaric converter, IEEE J. Oceanic Eng. 39 (2014) 386–397, http://dx.doi.org/10.1109/joe.2013.2260916.

[22] P.B.L. Neto, O.R. Saavedra, L.A. Souza Ribeiro, Optimization of electricity generation of a tidal power plant with reservoir constraints, Renew. Energy 81 (2015) 11–20, http://dx.doi.org/10.1016/j.renene.2015.03.011.

[23] P. Neto, O. Saavedra, L. Ribeiro, Analysis of a tidal power plant in the estuary of Bacanga in Brazil taking into account the current conditions and constraints, IEEE Trans. Sustain. Energy 8 (3) (2017) 1187–1194, http://dx.doi.org/10.1109/TSTE.2017.2666719.

[24] W. Geyer, R.C. Beardsley, S. Lentz, J. Candela, R. Limeburner, W. Johns, B. Castro, I. Soares, Physical oceanography of the Amazon shelf, Cont. Shelf Res. 16 (5–6) (1996) 575–616, http://dx.doi.org/10.1016/0278-4343(95)00051-8.

[25] C. Nittrouer, D. DeMaster, The Amazon shelf setting: Tropical, energetic, and influenced by a large river, Cont. Shelf Res. 16 (5–6) (1996) 553–573, http://dx.doi.org/10.1016/0278-4343(95)00069-0.

[26] J. Best, Anthropogenic stresses on the world's big rivers, Nat. Geosci. 12 (1) (2019) 7–21, http://dx.doi.org/10.1038/s41561-018-0262-x.

[27] F. Muller-Karger, C. McClain, P. Richardson, The dispersal of the Amazon's water, Nature 333 (6168) (1988) 56–59, http://dx.doi.org/10.1038/333056a0.

[28] O. Nikiema, J. Devenon, M. Baklouti, Numerical modeling of the Amazon river plume, Cont. Shelf Res. 27 (7) (2007) 873–899, http://dx.doi.org/10.1016/j.csr.2006.12.004.

[29] L. Stramma, J. Fischer, P. Brandt, F. Schott, Circulation, variability and near-equatorial meridional flow in the central tropical atlantic, in: G. Goni, P. Malanotte-Rizzoli (Eds.), Interhemispheric Water Exchange in the Atlantic Ocean, in: Elsevier Oceanography Series, vol. 68, Elsevier, 2003, pp. 1–22, http://dx.doi.org/10.1016/S0422-9894(03)80141-1.

[30] W.E. Johns, R.J. Zantopp, G.J. Goni, Cross-gyre transport by north Brazil current rings, in: G. Goni, P. Malanotte-Rizzoli (Eds.), Interhemispheric Water Exchange in the Atlantic Ocean, in: Elsevier Oceanography Series, vol. 68, Elsevier, 2003, pp. 411–441, http://dx.doi.org/10.1016/S0422-9894(03)80156-3.

[31] M. Dengler, F.A., C. Eden, P. Brandt, J. Fescher, R. Zantopp, Break-up of the Atlantic deep western boundary current into eddies at 8°S, Nature 432 (2004) 1018–1020, http://dx.doi.org/10.1038/nature03134.

[32] B. Knoppers, W. Ekau, A.G. Figueredo, The coast and shelf of east and northeast Brazil and material transport, Geo-Mar. Lett. 19 (1999) 171–178, http://dx.doi.org/10.1007/s003670050106.

[33] R. Fontes, B. Castro, R. Beardsley, Numerical study of circulation on the inner Amazon shelf, Ocean Dyn. 58 (2008) 187–198, http://dx.doi.org/10.1007/s10236-008-0139-4.

[34] R.C. Beardsley, J. Candela, R. Limeburner, W.R. Geyer, S.J. Lentz, B.M. Castro, D. Cacchione, N. Carneiro, The M2 tide on the Amazon shelf, J. Geophys. Res. 100 (C2) (1995) 2156–2202, http://dx.doi.org/10.1029/94JC01688.

[35] A.F. Shchepetkin, J.C. McWilliams, The regional ocean modeling system: A split-explicit, free-surface, topography following coordinates ocean model, Ocean Model. 9 (4) (2005) 347–404, http://dx.doi.org/10.1016/j.ocemod.2004.08.002.

[36] D.B. Haidvogel, H. Arango, W.P. Budgell, B.D. Cornuelle, E. Curchitser, E. Di Lorenzo, K. Fennel, W.R. Geyer, A.J. Hermman, L. Lanerolle, J. Levin, J.C. McWilliams, A.J. Miller, A.M. Moore, T.M. Powell, A.F. Shchepetkin, C.R. Sherwood, R.P. Signell, J.C. Warner, J. Wilkin, Ocean forecasting in terrain-following coordinates: Formulations ans skill assesment of the regional ocean modeling system, J. Comput. Phys. 227 (7) (2008) 3595–3624, http://dx.doi.org/10.1016/j.jcp.2007.06.016.

[37] D.B. Haidvogel, H.G. Arango, K. Hedstrom, A. Beckmann, P. Malanotte-Rizzoli, A.F. Shchepetkin, Model evaluation experiments in the North Atlantic Basin: Simulations in nonlinear terrain-following coordinates, Dyn. Atmospheres Oceans 32 (3–4) (2000) 239–281, http://dx.doi.org/10.1016/S0377-0265(00)00049-X.

[38] A. Shchepetkin, J. McWilliams, Quasi-monotone advection schemes based on explicit locally adaptive dissipation, Mon. Weather Rev. 126 (6) (1998) 1480–1541, http://dx.doi.org/10.1175/1520-0493(1998)126<1541:QMASBO>2.0.CO;2.

[39] A. Shchepetkin, J. McWilliams, A method for computing horizontal pressure-gradient force in an ocean model with a non-aligned vertical coordinate, J. Geophys. Res. 108 (C3) (2003) http://dx.doi.org/10.1029/2001JC001047.

[40] D.A. GLOBETaskTeam, Hastings, P.K. Dunbar, G.M. Elphingstone, M. Bootz, H. Murakami, H. Maruyama, H. Masaharu, P. Holland, J. Payne, N.A. Bryant, T.L. Logan, J.P. Muller, G. Schreier, J.S. MacDonald, The global land one-kilometer base elevation (GLOBE). Digital Elevation Model, 1999, Version 1.0, Digital data base on the World Wide Web, (URL: http://www.ngdc.noaa.gov/mgg/topo/globe.html) and CD-ROMs, NOAA–NGDC.

[41] Y. Le Bars, F. Lyard, C. Jeandel, L. Dardengo, The AMANDES tidal model for the Amazon estuary and shelf, Ocean Model. 31 (3–4) (2010) 132–149, http://dx.doi.org/10.1016/j.ocemod.2009.11.001.

[42] A.L. Aguiar, M. Marta-Almeida, L.O. Cruz, J. Pereira, M. Cirano, Forcing mechanisms of the circulation on the Brazilian equatorial shelf, Cont. Shelf Res. 247 (2022) 104811, http://dx.doi.org/10.1016/j.csr.2022.104811.

[43] HYCOM, Consortium for data assimilative modeling - HYCOM+NCODA Global Analysis, 2011, Available at: http://www.hycom.org/dataserver/glbanalysis/.

[44] P. Marchesiello, J.C. McWilliams, A. Shchepetkin, Open boundary conditions for long-term integration of regional oceanic models, Ocean Model. 3 (1–2) (2001) 1–20, http://dx.doi.org/10.1016/S1463-5003(00)00013-5.

[45] D. Chapman, Numerical treatment of cross-shelf open boundaries in a barotropic coastal ocean model, J. Phys. Oceanogr. 15 (8) (1985) 1060–1075, http://dx.doi.org/10.1175/1520-0485(1985)015.

[46] R. Flather, A tidal model of the northwest European continental shelf, 10 (6) (1976) 141–164, https://api.semanticscholar.org/CorpusID:222366586.

[47] G.D. Egbert, S.Y. Erofeeva, Efficient inverse modeling of barotropic ocean tides, J. Atmos. Oceanic Technol. 19 (2) (2002) 183–204, http://dx.doi.org/10.1175/1520-0426(2002)019<0183:EIMOBO>2.0.CO;2.

[48] S. Saha, S. Moorthi, H. Pan, X. Wu, J. Wang, S. Nadiga, P. Tripp, R. Kistler, J. Woollen, D. Behringer, H. Liu, D. Stokes, R. Grumbine, G. Gayno, J. Wang, Y. Hou, H. Chuang, H.H. Juang, J. Sela, M. Iredell, K.R. Treadon, D.P.V. Delst, D. Keyser, J. Derber, M. Ek, J. Meng, R.Y. H. Wei, S. Lord, H. van den Dool, A. Kumar, W. Wang, C. Long, M. Chelliah, Y. Xue, B. Huang, J. Schemm, W. Ebisuzaki, R. Lin, P. Xie, M. Chen, S. Zhou, W. Higgins, C. Zou, Q. Liu, Y. Chen, Y. Han, L. Cucurull, R.W. Reynolds, G. Rutledge, M. Goldberg, The NCEP climate forecast system reanalysis, Bull. Am. Meteorol. Soc. 91 (8) (2010) 1015–1058, http://dx.doi.org/10.1175/2010BAMS3001.1.

[49] A. Dai, T. Qian, K.E. Trenberth, J.D. Milliman, Changes in continental freshwater discharge from 1948 to 2004, J. Clim. 22 (10) (2009) 2773–2792, http://dx.doi.org/10.1175/2008JCLI2592.1.

[50] B. Bourlès, R. Lumpkin, M.J. McPhaden, F. Hernandez, P. Nobre, E. Campos, L. Yu, S. Planton, A. Busalacchi, A.D. Moura, J. Servain, J. Trotte, The PIRATA program: History, accomplishments, and future directions, Bull. Am. Meteorol. Soc. 89 (8) (2008) 1111–1126, http://dx.doi.org/10.1175/2008BAMS2462.1.

[51] T.M. Chin, J. Vazquez-Cuervo, E. Armstrong, A multi-scale high-resolution analysis of global sea surface temperature, Remote Sens. Environ. 200 (2017) 154–169, http://dx.doi.org/10.1016/j.rse.2017.07.029.

[52] M.I. Pujol, Y. Faugère, G. Taburet, S. Dupuy, C. Pelloquin, M. Ablain, N. Picot, DUACS DT2014: The new multi-mission altimeter data set reprocessed over 20 years, Ocean Sci. 12 (5) (2016) 1067–1090, http://dx.doi.org/10.5194/os-12-1067-2016.

[53] B. Jónsson, Harnessing Tidal Energy in the Westfjords (Masters Thesis), University of Akureyri, Akureyri, Iceland, 206p, 2010.

[54] J.W. Tester, E.M. Drake, M.J. Driscoll, M.W. Golay, W.A. Peters, Sustainable Energy: Choosing Among Options, second ed., The MIT Press, 2012, https://www.jstor.org/stable/j.ctt5hhbwk.

[55] J. Xia, R.A. Falconer, B. Lin, G. Tan, Estimation of annual energy output from a tidal barrage using two different methods, Appl. Energy 93 (2012) 327–336, http://dx.doi.org/10.1016/j.apenergy.2011.12.049.

[56] K.A. Samo, M.U. Keerio, S.A. Shaikh, A.R.H. Rigit, K.C. Mukwana, The energy output from the kuching barrage in east Malaysia, Eng. Technol. Appl. Sci. Res. 11 (2) (2021) 6970–6973, http://dx.doi.org/10.48084/etasr.4063.

[57] T. Adcock, S. Draper, Power extraction from tidal channels e multiple tidal constituents, compound tides and overtides, Renew. Energy 63 (2014) 797–806, http://dx.doi.org/10.1016/j.renene.2013.10.037.

[58] S. Neill, M. Hashemi, M. Lewis, The role of tidal asymmetry in characterizing the tidal energy resource of Orkney, Renew. Energy 68 (2014) 337–350, http://dx.doi.org/10.1016/j.renene.2014.01.052.